

Limb-Darkening Coefficients for the 4-Term and Power-2 Laws for the JWST Space Mission, Adopting PHOENIX Spherical Models at High Resolution *

NIRCam, NIRISS and NIRSpect passbands

A. Claret^{1,2}, P. H. Hauschildt³, and G. Torres⁴

¹ Instituto de Astrofísica de Andalucía, CSIC, Apartado 3004, 18080 Granada, Spain

² Dept. Física Teórica y del Cosmos, Universidad de Granada, Campus de Fuentenueva s/n, 10871, Granada, Spain

³ Hamburger Sternwarte, Gojenbergsweg 112, 21029 Hamburg, Germany

⁴ Center for Astrophysics | Harvard & Smithsonian, 60 Garden St., Cambridge, MA 02138, USA

Received; accepted;

ABSTRACT

Aims. Modeling observations of transiting exoplanets or close binary systems by comparing the observations with theoretical light curves requires precise knowledge of the distribution of specific intensities across the stellar disk. We aim to facilitate this type of research by providing extensive tabulations of limb-darkening coefficients for 11 frequently used near- and mid-infrared passbands on the NIRCam, NIRISS, and NIRSpect instruments installed on board the James Webb Space Telescope.

Methods. The calculation of the limb-darkening coefficients was based on spherically symmetric atmosphere models from the PHOENIX series, with high spectral resolution (approximately 10^6 wavelengths), and covering the wavelength range 0.1–6.0 μm . The models were computed for solar composition, and a microturbulent velocity of 1.0 km s^{-1} . We adopted two of the more accurate parametrizations for the coefficients: the 4-term law, and the power-2 law. We applied the Levenberg–Marquardt least-squares minimization method, with a strategy to determine the critical value μ_{crit} of the cosine of the viewing angle near the limb that is designed to improve numerical accuracy.

Results. The limb-darkening coefficients were derived based on a total of 306 atmosphere models covering an effective temperature range of 2400–7800 K, and a $\log g$ interval between 3.0 and 5.5. We discuss the quality of the fits to the specific intensities provided by the power-2 and 4-term laws, as well as by the often used quadratic law. Based on a comparison, we recommend the use of the 4-term or power-2 laws, in that order of preference.

Key words. stars: binaries: close; stars: evolution; stars: eclipsing binaries; stars: stellar atmospheres; planetary systems.

1. Introduction

Limb-darkening is an important phenomenon in several areas of Astrophysics research, including transiting extra-solar planets, eclipsing binary stars, spectroscopy, stellar microlensing events, interferometry, exozodiacal dust, line profiles of rotating stars, and many others. The correct treatment of this effect can be critical to the accuracy of the results, particularly in the present era of very high-precision observations made from space.

One of the first observations of the limb-darkening phenomenon was carried out centuries ago by Bouguer (1760). It was not until the beginning of the 20th Century that theoretical research into the limb-darkening phenomenon began, led by Schwarzschild (1906). This author introduced a linear law to describe the distribution of specific intensities as a function of a parameter $\mu = \cos \gamma$, where γ is the angle between the observer’s line of sight and the surface normal

(see also Milne 1921). That well-known linear equation is written as

$$\frac{I(\mu)}{I(\mu = 1)} = 1 - u(1 - \mu), \quad (1)$$

where $I(\mu)$ is the specific intensity as a function of position on the stellar disc, and u is the linear limb-darkening coefficient (LDC). Some four decades later, Chandrasekhar (1944) and Placzek (1947) worked out some results concerning limb-darkening for the grey atmosphere case.

A number of other laws with an extra term have been proposed since. For example, Kopal (1950) introduced the quadratic law

$$\frac{I(\mu)}{I(\mu = 1)} = 1 - a(1 - \mu) - b(1 - \mu)^2, \quad (2)$$

which has been quite popular in recent years. A decade later, Van’t Veer (1960) proposed the following equation for the grey case:

$$\frac{I(\mu)}{I(\mu = 1)} = 1 - b_1(1 - \mu) - b_3(1 - \mu)^3, \quad (3)$$

Send offprint requests to: A. Claret, e-mail: claret@iaa.es

* Tables 2 and 3 are only available at the CDS via anonymous ftp to cdsarc.u-strasbg.fr (130.79.128.5) or via <http://cdsarc.u-strasbg.fr/viz-bin/cat/J/A+A/XXX/XXX>

and KlingleSmith & Sobieski (1970) introduced the logarithmic law

$$\frac{I(\mu)}{I(\mu=1)} = 1 - e(1 - \mu) - f \mu \log(\mu). \quad (4)$$

Another bi-parametric equation, the square-root law by Díaz-Cordovés & Giménez (1992), has the expression

$$\frac{I(\mu)}{I(\mu=1)} = 1 - c(1 - \mu) - d(1 - \sqrt{\mu}). \quad (5)$$

Compared to the linear formula, these bi-parametric laws yielded improved agreement with the specific intensities provided by stellar atmosphere models, particularly in the case of Eq.(5) for stars with high effective temperatures. In the above equations, a , b_1 , e and c are the linear LDCs, while b is the quadratic LDC, b_3 the cubic LDC, f is the logarithmic LDC, and d the square-root LDC.

The best fit to model specific intensities provided by a bi-parametric law is due to Hestroffer (1997), who introduced a prescription that involves a power of μ , the so-called power-2 law. For a detailed discussion of the properties and advantages of this law, see Claret & Southworth (2022), their Sections 3 and 4. The power-2 law is expressed as

$$\frac{I(\mu)}{I(\mu=1)} = 1 - g(1 - \mu^h), \quad (6)$$

where g and h are the corresponding LDCs.

More recently, Claret (2000) proposed a 4-term non-linear law written as

$$\frac{I(\mu)}{I(1)} = 1 - \sum_{k=1}^4 a_k (1 - \mu^{\frac{k}{2}}), \quad (7)$$

in which a_k are the associated LDCs. So far, this 4-term limb-darkening prescription has achieved the best fits to the specific intensities from stellar atmosphere models, for both those using the plane-parallel and spherical geometry.

Finally, Sing et al. (2009) have advocated for an abbreviated form of the 4-term law given by

$$\frac{I(\mu)}{I(\mu=1)} = 1 - a_2(1 - \mu) - a_3(1 - \mu^{3/2}) - a_4(1 - \mu^2), \quad (8)$$

in which the $\mu^{1/2}$ term is omitted. Those authors pointed out that “The $\mu^{1/2}$ term from the four parameter non-linear law mainly affects the intensity distribution at small μ values, and is not needed when the intensity at the limb varies approximately linearly at small μ values”. We note, however, that not all atmosphere models show a quasi-linear drop in intensity near the limb, to a degree that warrants the omission of that term. Models with non-negligible curvature include those based on spherical geometry, or those for hot stars (see our comment above regarding Eq.(5), which does include the $\mu^{1/2}$ term).

The advent of space missions has come with tighter requirements on precision in dealing with the phenomenon of limb darkening. Until recently, this was a concern mostly at optical wavelengths, where the effect is more noticeable. However, the launch of the James Webb Space Telescope (JWST), at the end of 2021, represents a significant advancement, among others, in our ability to explore the properties of exoplanets in the near- and mid-infrared, a region

of the spectrum rich in new information. JWST has opened the door to detailed chemical studies of the complex atmospheres and compositions of these objects, through the analysis of light curves and/or transmission spectroscopy of unprecedented quality. These observations are now being gathered with the Near Infrared Camera (NIRCam), the Near Infrared Imager and Slitless Spectrograph (NIRISS), and the Near Infrared Spectrograph (NIRSpec) on board the spacecraft, as well as with the Mid Infrared Instrument (MIRI) at even longer wavelengths. To take full advantage of these new observations, proper treatment of limb-darkening and other effects has become more important. The main goal of this work, therefore, is to facilitate the above studies by providing the community with tabulations of coefficients for the limb-darkening laws that match the intensity distribution of state-of-the-art atmosphere models with the highest fidelity.

With that in mind, we begin in Sect. 2 by mentioning a few of the recent observational results concerning exoplanets using the above-mentioned instruments, where limb-darkening has played a role. We proceed then to Sect. 3, where we describe the stellar atmosphere models used to generate the LDCs, as well as the numerical method we applied. LDCs are presented here for some of the most used passbands of NIRCam, NIRISS, and NIRSpec. We end with Sect. 4, in which we comment briefly on the quadratic limb-darkening law — one of the more popular ones in the exoplanet field — and its limitations.

2. Advances in transmission spectroscopy and light curve analyses using JWST

A large number of papers making use of the instruments installed on board the JWST have appeared in the recent literature, and many more are sure to come. In the very active field of exoplanets, some of those studies have dealt with the analysis of transit light curves or phase curves, and others with transmission spectroscopy. In both cases they rely on limb-darkening laws, in one way or another. To illustrate some of that work, below is a list a few representative examples of such studies, along with the key results they have obtained:

- Rustamkulov et al. (2023) analyzed the exoplanet WASP-39b, of similar mass as Saturn, using the PRISM mode on JWST’s NIRSpec instrument. They reported the detection of the following chemical species in the atmosphere of the planet: Na (19σ), H₂O (33σ), CO₂ (28σ) and CO (7σ).
- Alderson et al. (2024) analyzed the super-Earth TOI-836b in the G395H passband of the NIRSpec instrument, and concluded that TOI-836b does not have an H₂ dominated atmosphere.
- Ahner et al. (2023) also investigated the exoplanet WASP-39b using NIRSpec/PRISM, and identified carbon dioxide (CO₂) in its atmosphere. The same study detected water vapor, and placed a limit on the abundance of methane. They also concluded that the atmospheric metallicity is between 1 and 100 times solar.
- Liu et al. (2025) studied the detectability of planetary oblateness, spin, and obliquity, from light curves obtained with NIRSpec/PRISM on JWST, using the exoplanet Kepler-167b as an example. They showed that observations of a single transit would be able to detect a Saturn-like oblateness ($f = 0.1$) with high confidence, or set a

stringent upper limit on the oblateness parameter, so long as the planetary spin is slightly misaligned ($\geq 20^\circ$) with respect to the orbital axis.

- Feinstein et al. (2023) reported an observation of the transmission spectrum of WASP-39b using the Single-Object Slitless Spectroscopy (SOSS) mode of the Near-Infrared Imager. From their analysis of the atmosphere, they estimated the metallicity to be in the range of 10–30 times solar. They found a sub-solar carbon-to-oxygen ratio, and a solar-to-super-solar potassium-to-oxygen ratio.

- Lustig-Yaeger et al. (2023) used NIRSpec in the G395H passband to validate and study the Earth-sized exoplanet LHS 475b. They ruled out primordial hydrogen-dominated and cloudless pure methane atmospheres.

- Wallack et al. (2024) investigated the spectrum of the sub-Neptune TOI-836c using the G395H passband of NIRSpec. The authors ruled out atmospheric metallicities below 175 times solar in the absence of aerosols at ≤ 1 millibar.

The above investigations, and many others like them that take advantage of the observational capabilities of the JWST mission, provide the motivation for supplying users with new LDCs for the 4-term and power-2 laws, covering 11 passbands used with the NIRCcam, NIRISS, and NIRSpec instruments. The limitations of other limb-darkening parametrizations have been pointed out in some of the above studies (e.g., Ahrer et al. 2023), and we expect the new coefficients calculated here to bring improvements in the analysis of observational data from this space mission.

3. Stellar atmosphere models and methodology

In this paper we make use of state-of-the-art spherically symmetric models based on the PHOENIX code (NewEra model grid; Hauschildt et al. 2025). A 1D spherically symmetric model may be described loosely as being made up of two parts: a core, and an envelope. Roughly speaking, the core behaves approximately as prescribed by a plane-parallel model. The envelope behaves differently, as it carries the spherical part. We define quasi-spherical models as those that do not consider the full intensity drop-off region. This concept is useful for situations in which small intensities near the limb coming from spherical models cannot be observationally detected, and/or if the effects of sphericity are negligible.

Here we employ the Levenberg–Marquardt least-squares minimization method (LML), adapted to the non-linear case to derive the LDCs for these models. Before applying the LML to each passband, the specific intensities for the photometric systems of interest were integrated using the following equation:

$$I_a(\mu) = (hc)^{-1} \frac{\int_{\lambda_1}^{\lambda_2} I(\lambda, \mu) \lambda S(\lambda)_a d\lambda}{\int_{\lambda_1}^{\lambda_2} S(\lambda)_a d\lambda}. \quad (9)$$

In this expression h is the Planck constant, λ is the wavelength, c is the speed of light in vacuum, $I_a(\mu)$ is the specific intensity in passband a , $I(\lambda, \mu)$ is the monochromatic specific intensity, and $S(\lambda)_a$ is the response function. Table 1 lists the JWST passbands considered for this work, and their mean wavelengths.¹

¹ The corresponding transmission functions for these and other JWST passbands may be obtained at <https://jwst-docs>.

Table 1: NIRCcam, NIRISS, and NIRSpec passbands.

Instrument and Passband	λ_a (μm)
NIRCcam F210M	2.10
NIRCcam F322W2	3.34
NIRCcam F444W	4.44
NIRISS SOSS Order 1	1.80
NIRISS SOSS Order 2	0.80
NIRISS F277W	2.80
NIRSpec G235H/F170LP	2.44
NIRSpec G235M/F170LP	2.45
NIRSpec G395H/F290LP	4.04
NIRSpec G395M/F290LP	4.03
NIRSpec PRISM	3.65

The LDC calculations were performed for a total of 306 PHOENIX models specifically computed for the present work, with each atmosphere model occupying more than 2.0 GB of disc space. In order to improve the input physics for the analysis of light curves and transmission spectroscopy, the models were originally computed at very high resolution, with approximately 1.08×10^6 wavelength points covering the range 0.1–6.0 μm that is relevant for the JWST passbands of NIRCcam, NIRISS, and NIRSpec. All models were calculated for the solar abundance and a fixed micro-turbulent velocity of $\xi = 1.0 \text{ km s}^{-1}$ (as per Hauschildt et al. 2025), over an interval in surface gravity $\log g$ between 3.0 to 5.5, and effective temperatures T_{eff} from 2400 K to 7800 K. In each case, we interpolated the original grid of 127 μ locations to form 60,000 regularly spaced points, in order to better sample the limb of the star and avoid numerical inaccuracies that would otherwise occur when using LML.

The specific intensities from spherical model atmospheres show a much more pronounced curvature near the limb than their plane-parallel model counterparts. In fact, the specific intensity for spherical models drops to zero. For this reason, it is more challenging to obtain good fits in that region with some of the simpler limb-darkening laws mentioned earlier. Only more flexible ones, such as the 4-term law, are able to provide acceptable fits for the entire intensity profile, although even for that prescription some of the passbands yield less than optimal fits (see, e.g., Fig. 1 by Claret et al. 2012).

In an earlier attempt to better describe the intensity distributions, Claret & Hauschildt (2003) introduced the concept of quasi-spherical models. However, this simple approach only takes into account the points in the intensity profile before the drop-off, down to an arbitrarily chosen value of μ referred to as the critical point, μ_{crit} , which is the smallest value used in fitting a given limb-darkening law. A year later, Wittkowski et al. (2004) introduced a more sophisticated approach, whereby instead of relying on an arbitrarily selected critical point, they defined it as the value of μ corresponding to the maximum of the derivative of the specific intensity with respect to r , where $r = \sqrt{1 - \mu^2}$. This point corresponds to a Rosseland mean optical depth

stsci.edu/jwst-exposure-time-calculator-overview/
[jwst-etc-pandea-engine-tutorial/](https://stsci.edu/jwst-etc-pandea-engine-tutorial/)
[jwst-etc-instrument-throughputs#gsc.tab=0](https://stsci.edu/jwst-etc-instrument-throughputs#gsc.tab=0), and plots can be generated at <https://jwst.etc.stsci.edu/>

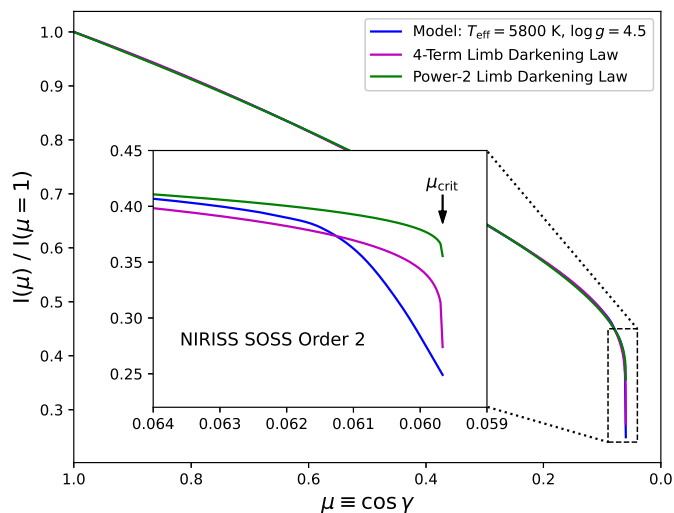


Fig. 1: Angular distribution of the specific intensity for a model with $T_{\text{eff}} = 5800$ K, $\log g = 4.5$, $[M/H] = 0.0$, and $\xi = 1.0$ km s $^{-1}$ (blue line), for the NIRISS SOSS Order 2 passband. The fits provided by the 4-term and power-2 laws are displayed for comparison. The inset shows an enlargement around the drop-off region.

$\tau_R \approx 1.0$. The present PHOENIX models were computed with sufficient μ sampling in the drop-off region to allow us to determine the required derivative more precisely. Here we adopt the methodology of Wittkowski et al. (2004), which produces steeper profiles and is therefore more difficult to adjust, but provides a better representation of the spherical part of the atmosphere models. The merit function used as a measure of the quality of the fit for each passband is

$$\chi^2 = \sum_{i=1}^N (y_i - Y_i)^2, \quad (10)$$

where y_i is the model intensity at point i , Y_i is the fitted function at the same point, and N is the number of μ points.

The limb-darkening coefficients calculated for the 4-term law are presented in Table 2 for all passbands, and those for the power-2 law in Table 3. Both are available at the CDS.

As an illustration, Fig. 1 and Fig. 2 present comparisons of the fits to the intensity profile for the 4-term and the power-2 laws, for two of the NIRISS passbands. Plots for the other passbands in Table 1 are similar. In general, the fits with the 4-term law give smaller χ^2 values than those with the power-2 law. In some cases the χ^2 values from the 4-term law can be up to 100 times smaller, while in others they are similar. A graphical comparison of the fit qualities between the 4-term, power-2, and quadratic laws is shown in Figs. 3–5.

4. Final remarks

Among the bi-parametric limb-darkening laws, the quadratic formula (Eq. 2) is one of the most commonly used in the literature for the analysis of light curves and transmission spectroscopy. We point out, however, that this prescription generally does not provide accurate fits to the

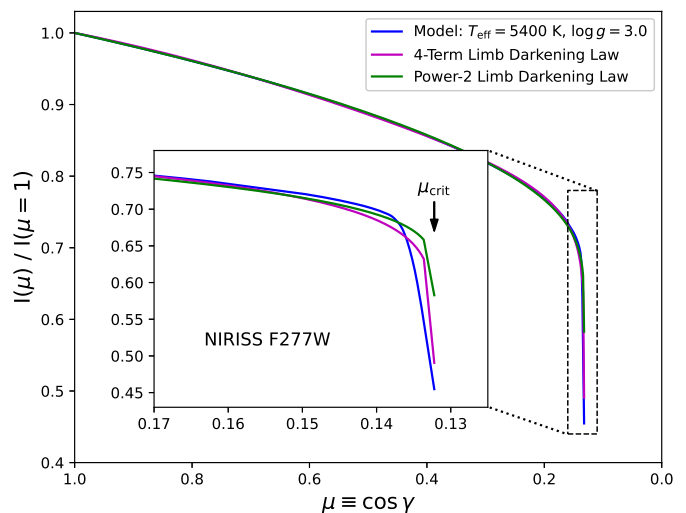


Fig. 2: Similar to Fig. 1, for a model with $T_{\text{eff}} = 5400$ K, $\log g = 3.0$, $[M/H] = 0.0$, and $\xi = 1.0$ km s $^{-1}$ (blue line). The NIRISS passband shown here is F277W.

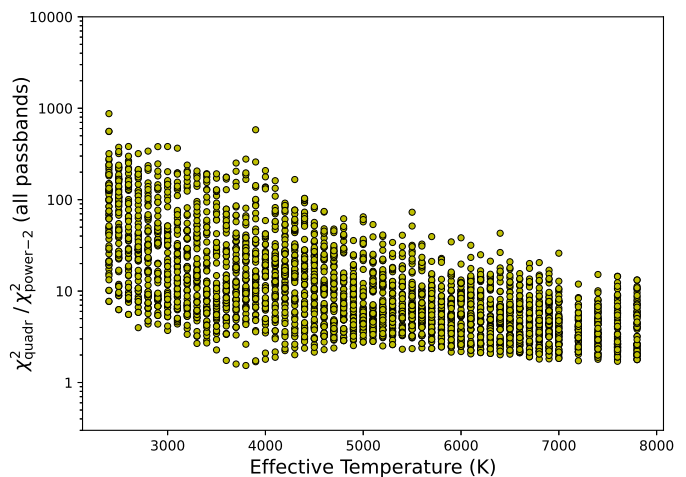


Fig. 3: Comparison of the quality of the fits for all passbands studied here. The quality metric shown is the ratio between the χ^2 values computed using the quadratic law and the power-2 law, for all 306 models.

specific intensities produced by realistic atmosphere models, for any given T_{eff} , $\log g$, or metallicity. This is the case even for models that adopt plane-parallel geometry (Claret & Southworth 2022; see their Figs. 2 and 3). The χ^2 values associated with such fits are quite high, and the flux is not conserved within reasonable limits. See Figs. 3–5, where we compare the qualities of the fits among the quadratic, power-2, and 4-term laws. Use of the quadratic prescription runs the risk of implicitly introducing into the analysis a model of the stellar atmosphere that is not a good representation of the one intended to begin with, characterized by certain values of T_{eff} , $\log g$, metallicity, and microturbulent velocity. As a result, significant biases can be introduced into the analysis of high-precision data such as JWST provides. Similar comments have been made recently by Coulombe et al. (2024). In reality, of course, none of the three laws mentioned previously (4-term, power-2,

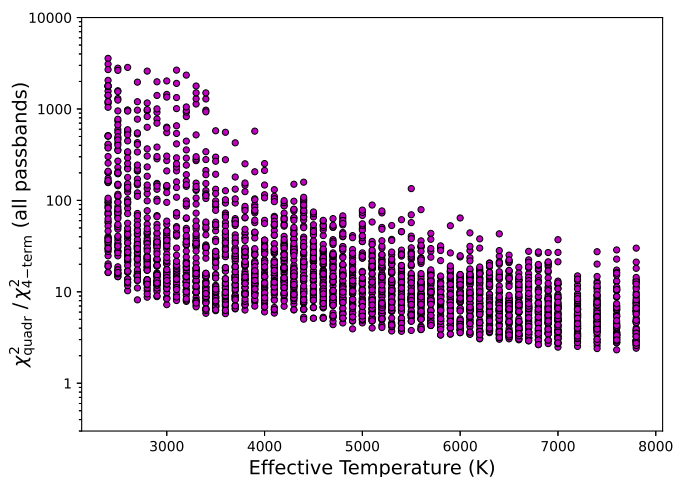


Fig. 4: Similar to Fig. 3, for the ratio between the χ^2 values computed using the quadratic law and the 4-term law.

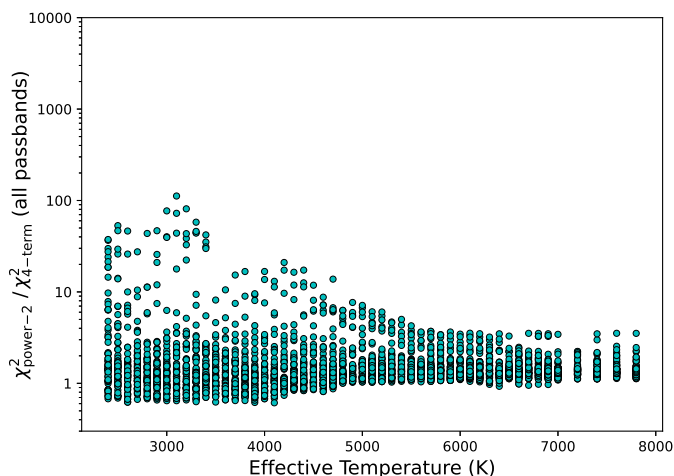


Fig. 5: Similar to Fig. 3, for the ratio between the χ^2 values computed using the power-2 law and the 4-term law.

quadratic) achieve a perfect fit to the distribution of specific intensities, as they are only convenient approximations. However, based on the results of this paper, and others discussing limb-darkening, it is advisable to avoid using the quadratic law. Instead, here we recommend the 4-term or power-2 laws, in that order of preference. The LDCs computed in this work for the 11 JWST passbands are available at the CDS: Table 2 (4-term formula) and Table 3 (power-2 formula). Additional calculations can be carried out on request for other photometric systems that are within the mentioned spectral range of the present models.

5. Data availability section

Tables 2 and 3 are only available in electronic form at the CDS via anonymous ftp to [cdsarc.u-strasbg.fr](ftp://cdsarc.u-strasbg.fr) (130.79.128.5) or via <http://cdsweb.u-strasbg.fr/cgi-bin/qcat?J/A+A/>.

References

- Alderson, L., Batalha, N. E., Wakeford, H. R. et al., 2024, *AJ*, 167, 216
- Ahrer, E.-M., Alderson, L., Batalha, N. M. et al., 2023a, *Nature*, 614, 649
- Ahrer, E.-M., Stevenson, K. B., Mansfield, M. et al., 2023b, *Nature*, 614, 653
- Bouguer, P., 1760, *Traité d’Optique*, l’Abbé de la Caille, Paris
- Chandrasekhar, S., 1944, *ApJ*, 99, 180
- Claret, A., 2000, *A&A*, 363, 1081
- Claret, A., Hauschildt, P. H., 2003, *A&A* 412, 241
- Claret, A., Hauschildt, P. H., Witte, S. 2012, *A&A*, 546, 14
- Claret, A., Southworth 2022, *A&A*, 664, A128
- Coulombe, L.-P., Roy, P.-A., & Benneke, B. 2024, *AJ*, 168, 227
- Díaz-Cordovés, J., Giménez, A., 1992, *A&A*, 259, 227
- Feinstein, A. D., Radica, M., Welbanks, L. et al., 2023, *Nature*, 614, 670
- Hauschildt, P. H., Barman; T., Baron, E. et al., 2025, *A&A*, in press (arXiv:2504.17597)
- Hestroffer, D., 1997, *A&A*, 327, 199
- Klinglesmith, D. A., Sobieski, S., 1970, *AJ*, 75, 175
- Kopal, Z., 1950, *Harvard College Observatory Circular*, 454, 1
- Liu, Q., Zhu, W., Zhou, Y. et al., 2025, *AJ*, 169, 79
- Lustig-Yaeger, J., Fu, G., May, E. M., 2023, *Nature Astronomy*, 7, 1317
- Milne, E. A., 1921, *MNRAS*, 81, 361
- Placzek, G. 1947, *Phys. Rev.* 72, 556
- Rustamkulov, Z., Sing, D. K., Mukherjee, S. et al., 2023, *Nature*, 614, 659
- Sing, D. K., Désert, J., Lecavelier Des Etangs, A. et al., 2009, *A&A*, 505, 891
- Schwarzschild, K., 1906, *Nachrichten von der Gesellschaft der Wissenschaften zu Göttingen, Mathematisch-Physikalische Klasse*, p. 43
- Van’t Veer, F., 1960, *Rech. Astr. Obs. Utrecht* 14, No. 3
- Wallack, N. L., Batalha, N., Alderson, L. et al., 2024, *AJ*, 168, 77
- Wittkowski, M., Aufdenberg, J. P., Kervella, P., 2004, *A&A*, 413, 711

Acknowledgements. We thank the anonymous referee for helpful comments. The Spanish MINC/AEI (PID2022-137241NB-C43 and PID2019-107061GB-C64) are gratefully acknowledged for their support during the development of this work. We also thank R. Morales and N. Robles (UDIT-IAA-CSIC) for their assistance with the calculations. AC also acknowledges financial support from grant CEX2021-001131-S, funded by MCIN/AEI/10.13039/501100011033. The model grid calculations presented here were partially performed at the National Energy Research Supercomputer Center (NERSC), which is supported by the Office of Science of the U.S. Department of Energy under Contract No. DE-AC03-76SF00098. The authors gratefully acknowledge the computing time made available to them on the high-performance computers HLRN-IV at GWDG at the NHR Center NHR@Göttingen and at ZIB at the NHR Center NHR@Berlin. These Centers are jointly supported by the Federal Ministry of Education and Research, and the state governments participating in the NHR (www.nhr-verein.de/unsere-partner). Additional computing time was provided by the RRZ computing clusters Hummel and Hummel2. We thank all of these institutions for a generous allocation of computer time. This research has made use of the SIMBAD database, operated at the CDS, Strasbourg, France, and of NASA’s Astrophysics Data System Abstract Service.